Hidden spin-order-induced room-temperature ferroelectricity in a peculiar conical magnetic structure

Shi-Peng Shen,[1] Xin-Zhi Liu,[2] Yi-Sheng Chai,[1,*] Andrew Studer,[3] Kirrily Rule,[3] Kun Zhai,[1] Li-Qin Yan,[1] Da-Shan Shang,[1] Frank Klose,[3,4] Yun-Tao Liu,[2] Dong-Feng Chen,[2] and Young Sun[1,5,*]

[1]*Beijing National Laboratory for Condensed Matter Physics, Institute of Physics, Chinese Academy of Sciences, Beijing 100190, China*
[2]*Department of Nuclear Physics, China Institute of Atomic Energy, Beijing 102413, China*
[3]*Australian Centre for Neutron Scattering, Australian Nuclear Science and Technology Organization, Lucas Heights, New South Wales 2234, Australia*
[4]*Department of Physics and Materials Science, The City University of Hong Kong, Hong Kong, China*
[5]*School of Physical Science, University of Chinese Academy of Sciences, Beijing 100190, China*

(Received 7 December 2016; published 7 March 2017)

A novel mechanism of spin-induced ferroelectricity is unraveled in the alternating longitudinal conical (ALC) magnetic structure. Because the noncollinear ALC structure possesses a *c*-axis component with collinear ↑–↑–↓–↓ spin order, spin-driven ferroelectricity along the *c* axis due to the exchange striction mechanism is predicted. Our experiments verify this prediction in the Y-type hexaferrite $Ba_{0.3}Sr_{1.7}Co_2Fe_{11}AlO_{22}$, where ferroelectricity along the *c* axis is observed up to room temperature. Neutron diffraction data clearly reveal the ALC phase and its evolution with magnetic fields. The *c*-axis electric polarization can be well modulated by applying either *ab*-plane or *c*-axis magnetic fields, even at 305 K. This kind of spin-induced ferroelectricity associated with the ALC magnetic structure provides a new resource of type II multiferroics.

DOI: 10.1103/PhysRevB.95.094405

I. INTRODUCTION

Spin-order-induced multiferroics, where the space inversion symmetry is broken by magnetic structures, have attracted unprecedented interests in the last decade, because of their large magnetoelectric (ME) coupling effects and great potential for numerous applications [1–5]. In those materials, either collinear or noncollinear spin textures can induce ferroelectric (FE) polarization (P) by breaking the centrosymmetry. For example, the noncollinear cycloidal and conical spin orders break the centrosymmetry and induce ferroelectricity in $TbMnO_3$ [1] and $CoCr_2O_4$ [6], respectively, while in *o*-$HoMnO_3$ [7–9] and $Ca_3(Co,Mn)_2O_6$ [10], the so-called ↑–↑–↓–↓ collinear spin structure can also generate ferroelectricity by removing the space inversion operation. Several microscopic mechanisms have been proposed to explain the generation of the spin-driven ferroelectricity. The spin-current model (the Katsura-Nagaosa-Balatsky [KNB] model) [11] or inverse Dzyaloshinskii-Moriya (DM) interaction [12], is often used to explain noncollinear spin-induced ferroelectricity, where $\boldsymbol{P} \propto \Sigma \boldsymbol{k} \times (\mu_i \times \mu_j)$ ($\boldsymbol{k}$ is the magnetic wavevector and $\boldsymbol{\mu}_i$ and $\boldsymbol{\mu}_j$ are magnetic moments at the adjacent lattice sites). However, the exchange striction mechanism [10,13] is believed to be responsible for spin-driven ferroelectricity in collinear spin configurations, where $P \propto \sum \boldsymbol{\mu}_i \cdot \boldsymbol{\mu}_j$. In rare cases, the exchange striction mechanism could also play a dominant role in noncollinear spin structures. Meanwhile, as spin-induced ferroelectricity was often observed at cryogenic temperatures [1,6–10], it is important to find novel magnetic structures that break centrosymmetry to induce P and enable ME coupling at room temperature. In this paper, we present such an intriguing example of room-temperature ferroelectricity induced by the exchange striction mechanism in a peculiar conical spin structure.

*Corresponding authors: yschai@iphy.ac.cn; youngsun@iphy.ac.cn

Hexaferrites that involve strongly frustrated superexchange interactions between Fe^{3+} ions and host many noncollinear conical spin orders are the most promising materials of spin-order-driven multiferroics in a wide temperature range [14–23]. In these multiferroic hexaferrites, P is normally induced by the transverse conical (TC) noncollinear spin order in the hexagonal plane (*ab* plane), which can be well interpreted by the KNB model [19]. Ferroelectricity along the *c* axis has never been reported in them. Nevertheless, in addition to the TC spin order, there are other conical spin configurations in hexaferrites. Specifically, the alternating longitudinal conical (ALC) order can break the space inversion symmetry because its *c*-axis spin component happens to form the ↑–↑–↓–↓ collinear order. As we mentioned above, the ↑–↑–↓–↓ collinear spin structure can generate ferroelectricity via the exchange striction mechanism [10]. Therefore, an extra ferroelectricity along the *c* axis is expected in the ALC phase.

To verify this prediction, we have performed a careful study in the Y-type hexaferrite $Ba_{0.3}Sr_{1.7}Co_2Fe_{11}AlO_{22}$ (BSCFAO) single crystal in which the ALC phase exists even above room temperature, as confirmed by neutron diffraction measurements. Ferroelectricity along the *c* axis, as well as ME coupling, is observed up to 305 K, supporting the new mechanism of spin-induced ferroelectricity associated with the ALC phase.

The Y-type hexaferrites have a general chemical formula of $Ba_xSr_{2-x}Me_2Fe_{12}O_{22}$ ($Me = Zn^{2+}, Co^{2+}, Mg^{2+}$, *etc.*) with the $R\text{-}3m$ space group. Their magnetic structure can be viewed as the alternate stacks of large (L) and small (S) blocks along the *c* axis, as shown in Fig. 1(a). Within each block, the magnetic moments of metal ions (Fe^{3+} and Me^{2+}) are ferrimagnetically aligned and yield a large magnetic moment $\boldsymbol{\mu}_L$ on the L block and a small moment μ_S on the S block [24]. Due to the different magnetic anisotropies in the L and S blocks and the magnetic frustration at the block boundaries, this system tends to develop a helical or conical spin order with

 ©2017 American Physical Society

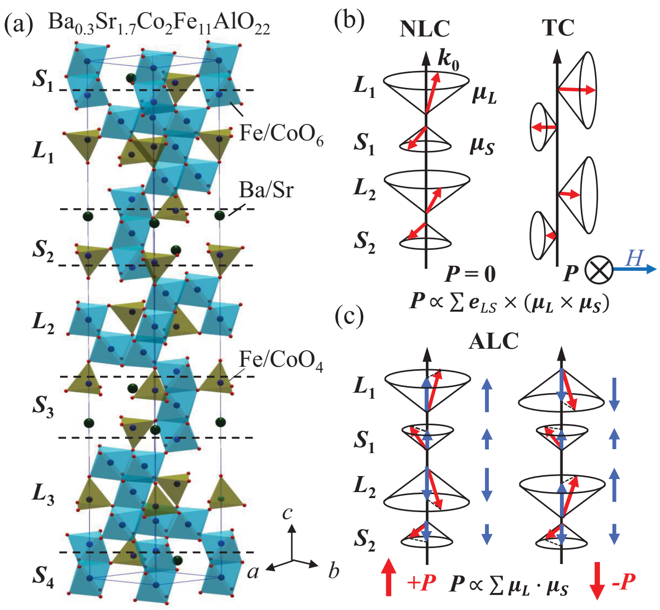

FIG. 1. (a) The crystal and magnetic structure of Y-type hexaferrites. The magnetic structure can be viewed as alternating S and L blocks stacked along the c axis. (b) and (c) The schematic illustration of different conical magnetic structures: (b) NLC and TC and (c) ALC.

a wavevector $\boldsymbol{k}$ along the c axis. According to previous papers [25–28], almost all multiferroic Y-type hexaferrites, like $Ba_2Mg_2Fe_{12}O_{22}$ and $Ba_{0.5}Sr_{1.5}Zn_2(Fe_{0.92}Al_{0.08})_{12}O_{22}$, possess longitudinal conical (LC) spin configurations after zero magnetic field cooling, which are paraelectric (PE) without breaking the centrosymmetry. However, when an in-plane magnetic field (H_{ab}) is applied, the spin configuration would be driven into the so-called commensurate TC phases, which are FE phases with the in-plane polarizations $P_{ab} \perp H_{ab}$ based on the KNB model, as seen in the right panel of Fig. 1(b). Previous neutron diffraction results suggest that there are two types of LC magnetic structure in Y-type hexaferrites [26,28,29]: the c component of magnetic moments ferrimagnetically aligned, or the normal longitudinal cone (NLC) [Fig. 1(b)], and antiferromagnetically aligned, or the ALC [Fig. 1(c)]. For the ALC phase, an ↑–↑–↓–↓ magnetic arrangement along the c axis is combined with an in-plane helical order. We noticed that the hidden ↑–↑–↓–↓ component breaks the space inversion symmetry and induces a polar axis along c direction. Therefore, an electric polarization is expected along the c axis (P_c) in this ALC phase (see the description and Fig. S1 in the Supplemental Material [30]).

II. EXPERIMENTS

Single crystals of BSCFAO were grown from the Na_2O-Fe_2O_3 flux in air [31]. The as-grown crystals were annealed in O_2 atmosphere at 900 °C for 16 days to reduce oxygen vacancies and enhance the resistivity. The neutron diffraction measurements ($\lambda = 2.41$ Å) were performed at high-intensity diffractometer WOMBAT in Australian nuclear science and technology organization (ANSTO). The sample was aligned first in $h0l$ plane and then $hk0$ plane; accordingly, a vertical magnetic field was applied first in ab plane and then along c axis. For the $H//c$-axis configuration, we utilized the vertical span range of WOMBAT two-dimensional (2D) position sensitive detector (PSD), which allows us to observe out-of-plane reflections with nonzero l ($-2 < l < 3$), taking advantage of the very small reciprocal spacing unit along c axis. These two configurations enable us to monitor both in-plane and c-axis spin-order evolution at various magnetic fields and temperatures.

The magnetic measurements were performed in the Magnetic Properties Measurement System (MPMS, Quantum Design). All electrical measurements were carried out in a cryogen-free superconducting magnet system (Oxford Instruments, Teslatron PT) with a homemade probe. The dielectric constant was measured by an Agilent 4980A inductance-capacitance-resistance (LCR) meter. The ME current was recorded by a Keithley 6517B electrometer. Before the ME current measurements, the specimen was prepoled by the electric field from the high magnetic field PE phase into the low field FE phase, unless stated otherwise. After removing the poling electric field, the ME currents were then measured with either increasing or decreasing H to the PE phase again.

III. RESULTS AND DISCUSSION

The temperature dependence of magnetization and the neutron diffraction pattern, plotted in Fig. 2, illustrates the zero

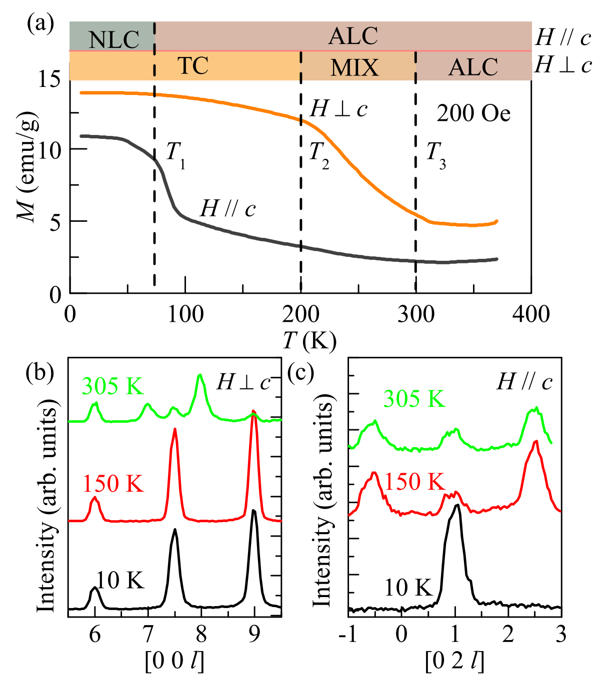

FIG. 2. (a) Temperature dependence of magnetization and the schematic magnetic phase diagram of BSCFAO with $H = 200$ Oe applied parallel or perpendicular to the c axis. (b) and (c) Neutron diffraction patterns of BSCFAO in zero magnetic field at selected temperatures. The data were collected after removing the high magnetic field $H_{ab} = 70$ kOe or $H_c = 70$ kOe at 10 K. The relative bad resolution for $H//c$ in (c) corresponds to the vertical focusing of the incident neutron beam.

field states of BSCFAO after the high-H history. For the M-T measurements, the magnetic fields were first applied to 70 kOe at 10 K and then ramped down to 200 Oe; subsequently, the M-T curves were measured during warming between 10 and 370 K, as shown in Fig. 2(a). The nature of these phases could be revealed by using the neutron-diffraction method. The nuclear Bragg peaks, $\mathbf{Q}_N$, should satisfy the reflection condition $-h + k + l = 3n$; the rest peaks are purely due to magnetic orders. In addition, only the spin components perpendicular to $\mathbf{Q}_N$ can be observed by neutron diffraction. For $H \perp c$-axis configuration, the in-plane M slowly decreases at low temperature, undergoes a dramatic drop around $T_2 \sim 200$ K, and becomes flat about 300 K. The magnetic phase below T_2 should correspond to a commensurate TC phase, which has been observed in some Y-type hexaferrites at low temperature [23,25]: the zero field phase can be changed by the in-plane H history from the incommensurate LC phases into a metastable commensurate TC phase, which is also evidenced by our M-H curve and neutron diffraction results at 10 K (see Fig. S2 in the Supplemental Material [30]).

The neutron diffraction along [00l] direction, plotted in Fig. 2(b), clearly shows that the commensurate peaks at $\mathbf{Q} = \mathbf{Q}_N \pm \boldsymbol{k}_1 = \mathbf{Q}_N \pm 3(0\,0\,1/2)$ are visible below T_2. Since the associated spin components are perpendicular to the c axis, this indicates that the commensurate TC phase is preserved, similar to the result in Ref. [31]. At 305 K, the $\boldsymbol{k}_1$ peak along [00l] almost disappears; meanwhile, two broad incommensurate peaks at $\mathbf{Q} = \mathbf{Q}_N \pm \boldsymbol{k}_2 = \mathbf{Q}_N \pm 3(0\,0\,\delta)(\delta \sim 0.33)$ appear, which means that the TC phase cannot be maintained and returns to the incommensurate LC phase. For $H//c$ configuration, the M-T curve is almost flat below 50 K and experiences an abrupt decrease around $T_1 = 70$ K. This behavior is a typical magnetic phase transition for Y-type hexaferrites from NLC to ALC phase [26], which is confirmed by our neutron diffraction results [Fig. 2(c)]. Both (1 0 l/2) and (0 2 l/2) reflections are observed to exhibit the same behavior simultaneously. For simplicity, we only show the (0 2 l/2) peaks in Fig. 2(c). The only visible peak at 10 K is at (0 2 1), which is the nuclear or ferromagnetic component Braggs peak, and no trace of the incommensurate diffraction peak for the ab-plane magnetic component can be observed along [02l] at 305 K. This indicates that the associated magnetic component for the diffraction direction [02l] is parallel to c axis. Above T_1, antiferromagnetic peaks appear at $\mathbf{Q} = \mathbf{Q}_N \pm \boldsymbol{k}_1 = (0\,2\,1) \pm 3(0\,0\,1/2)$; therefore, we can conclude the phase above T_1 is ALC for $H//c$ configuration. The magnetic phase diagrams for both $H \perp c$ and $H//c$ configurations are summarized in Fig. 2(a). The LC phase for $H \perp c$ above T_3 should be a pure ALC instead of the NLC phase, since only the ALC phase is expected to stabilize near the zero field at high temperatures after an out-of-plane H history.

To verify that the ALC spin order can induce the c-axis polarization, systematic ME measurements on the BSCFAO were performed with the E and $H//c$ configuration at 150 K, since the ALC phase is expected near the zero field above T_1 in such field configurations [Fig. 2(a)]. Figures 3(a)–3(d) displays the H_c dependence of the relative change in dielectric constant $\Delta\varepsilon(H) = [\varepsilon(H) - \varepsilon(0)]/\varepsilon(0)$, electric polarization (P_c), magnetization (M_c), and the neutron diffraction for BSCFAO at 150 K. As illustrated in Fig. 3(a), the $\Delta\varepsilon_c$ curves show

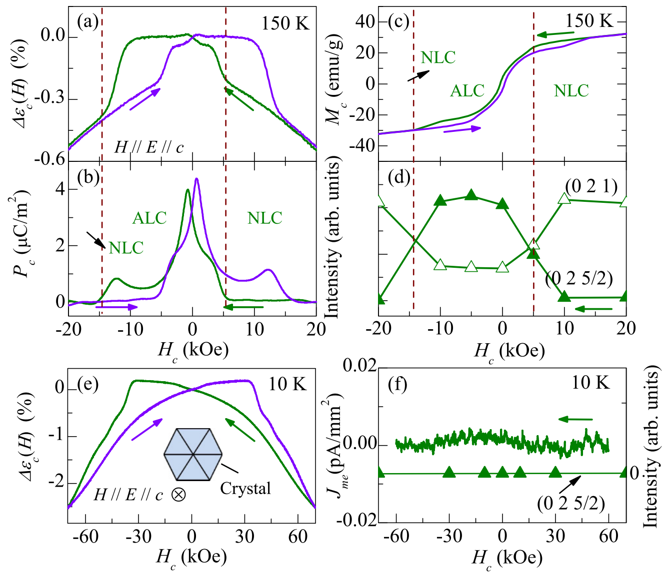

FIG. 3. H_c dependence of (a) dielectric constant $\Delta\varepsilon_c$, (b) electric polarization P_c, (c) magnetization M_c, and (d) neutron diffraction intensity at 150 K. H_c dependence of (e) $\Delta\varepsilon_c$ and (f) ME current J_{me} and neutron diffraction intensity at 10 K.

stepwise plateau features near zero H_c. These features can be attributed to the expected P_c of the ALC phase, verified by the H_c-dependent P_c curve in Fig. 3(b). Moreover, the sign of P_c can be reversed by $-E$ poling (see Fig. S3 in the Supplemental Material [30]), indicating that the ALC phase is a FE phase.

The H_c-dependent P_c and $\Delta\varepsilon_c(H)$ clearly trace out a FE phase centered on zero H, and P_c becomes zero for $|H_c| > 10$ kOe, as shown in Fig. 3(b). In addition, the saturation of M_c and the disappearance of P_c happen in the same field scale, indicating that the high H_c can destroy the ALC phase and lead to a non-FE NLC phase, which is confirmed by the neutron diffraction results [Fig. 3(d)]: At $H_c = 10$ and 20 kOe, only the ferromagnetic peak at $\mathbf{Q}_N = (0\,2\,1)$ is visible along (0 2 l) direction, implying the NLC phase at high H_c. This observation also holds for (1 0 l), (1, 1, l), and (1 3 l) directions, which confirms the magnetic scattering is contributed from the c-axis component. As H_c is ramped down to 5 kOe, the intensity of ferromagnetic peak $\mathbf{Q}_N$ sharply decreases; meanwhile, the new $\boldsymbol{k}_1$ antiferromagnetic peaks [$\mathbf{Q} = \mathbf{Q}_N \pm \boldsymbol{k}_1 = (0\,2\,1) \pm 3(0\,0\,1/2)$] appear at the same field, indicating the transition from the NLC to ALC phase. As we can see, the FE phase and ALC magnetic phase share the same boundary at both negative and positive H_c, meaning that the P_c is induced by the ALC phase. Since both FE ALC and PE NLC phases possess the spiral spin order in the ab plane, the only difference between them is whether the hidden ↑–↑–↓–↓ spin order along the c axis exists [Fig. 1(c)]. We can conclude that the P_c originates from the hidden ↑–↑–↓–↓ spin order in the ALC phase via exchange striction mechanism (see discussion in the Supplemental Material [30]).

Instead of ALC, the NLC phase appears in low H_c field at 10 K, as seen in Fig. 2(a). Therefore, no P_c should be expected at 10 K as the space inversion symmetry is preserved in the NLC phase. As shown in Fig. 3(e), the $\Delta\varepsilon_c(H)$-H_c curve at 10 K shows distinctive dielectric features compared with those at

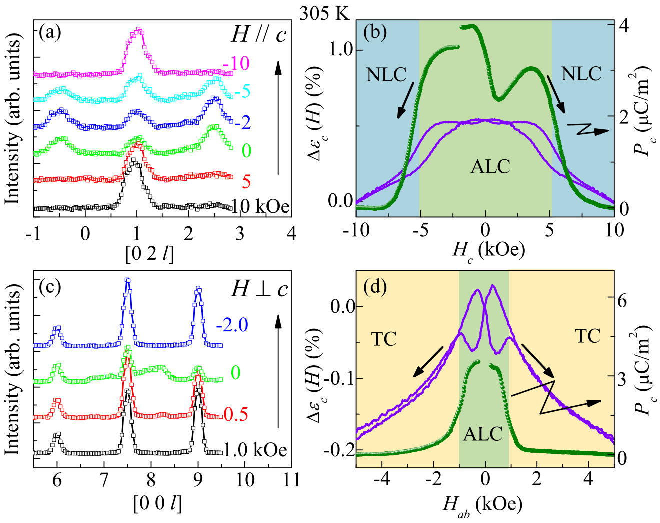

FIG. 4. H_c dependence of (a) the neutron diffraction pattern and (b) $\Delta\varepsilon_c$ and electric polarization P_c at 305 K. H_{ab} dependence of (c) the neutron diffraction pattern and (d) $\Delta\varepsilon_c$ and electric polarization P_c at 305 K.

150 K. No stepwise dielectric plateau (marking the FE phase at 150 K) can be observed in the H_c region measured. In addition, ME current J_{me} is practically zero within the resolution of the instrument. The absence of P_c at 10 K can be explained by the neutron diffractions at 10 K, as plotted in Fig. 3(f). The intensity for the antiferromagnetic $\boldsymbol{k}_1$ peak [$\mathbf{Q} = \mathbf{Q}_N \pm \boldsymbol{k}_1 = (0\,2\,1) \pm 3(0\,0\,1/2)$] is always zero from -70 to 70 kOe, indicating only the NLC phase exists for $H//c$ at 10 K. That confirms that P_c cannot appear in the NLC phase.

Since the ALC phase can persist up to room temperature for both $H//c$ and $H//ab$ configurations according to the phase diagram in Fig. 2(a), the modulation of P_c by H_c or H_{ab} should be achieved at room temperature. Figure 4(a) presents the H_c dependence of neutron diffraction at 305 K: only the ferromagnetic $\mathbf{Q}_N$ peak is visible at $H_c = 5$ and 10 kOe. Then, ramping the H_c to zero, the intensity of the $\mathbf{Q}_N$ peak gradually decreases and the antiferromagnetic $\boldsymbol{k}_1$ peak appears. At -10 kOe, the ferromagnetic $\mathbf{Q}_N$ peak is fully recovered. This reveals that the ALC phase still dominates near zero H_c and is replaced by the NLC phase at high H_c field at 305 K. The dielectric behavior is also exhibiting the stepwise plateau feature at high H_c, similar to those at 150 K. Due to current leakage at 305 K, we chose to electrically pole the sample at -10 kOe and then ramp H_c to -2 kOe to drive the BSCFAO into the ALC phase. After these procedures, E_c was removed, and J_{me} was measured during the H_c increasing (positive H_c region) and decreasing (negative H_c region) run. The P_c-H_c plot obtained by integrating J_{me} with time [Fig. 4(b)], clearly demonstrates the room-temperature ME effect due to the modulation on the ALC phase.

Then, we further explored the modulation of P_c by H_{ab} at 305 K. Since H_{ab} can drive the ALC phase into the TC phase, where a finite P_{ab} is induced (see Fig. S4 in the Supplemental Material [30]), P_c would become zero in high H_{ab}. Figure 4(c) explicitly shows the H_{ab}-dependent change of the Bragg peaks along [00l] during H_{ab} ramping from 10 to -10 kOe. At $H_{ab} = 10$ kOe, the commensurate $\boldsymbol{k}_1$ peaks along [00l] are clearly visible, indicating that the associated spin order is the TC phase. When H_{ab} is reduced below 2 kOe, the $\boldsymbol{k}_1$ peak sharply decreases and incommensurate $\boldsymbol{k}_2$ peaks appear. This indicates that the system returns to the ALC phase. Further ramping H_{ab} to negative field, the incommensurate $\boldsymbol{k}_2$ peaks disappear again, and the sample reenters the TC phase. The P_c-H_{ab} curve, plotted in Fig. 4(d), shows that P_c is about 4 μC/m^2 in the ALC phase, comparable with the magnitude of P_c with $H//c$, and becomes zero in the high H_{ab} field region. Moreover, two dielectric peaks ($\Delta\varepsilon_c = [\varepsilon(H) - \varepsilon(0)]/\varepsilon(0)$) at low H_{ab} are observed, confirming the transitions of PE to FE phase or *vice versa* under $H \perp c$ configuration. This further proves that the P_c cannot exist in the TC phase and only originates from the ALC phase.

IV. CONCLUSION

In summary, our paper discloses a new resource of spin-induced ferroelectricity: the collinear ↑–↑–↓–↓ spin order can be hidden in the noncollinear ALC phase and produces ferroelectricity via the exchange striction mechanism. This leads to room-temperature ferroelectricity and ME effects in the Y-type hexaferrite BSCFAO. The hidden ↑–↑–↓–↓ spin-order-induced electric polarization provides a new pathway to seek novel type II multiferroics and may be further explored in other conical helimagnets to yield advanced multiferroics at room temperature.

ACKNOWLEDGMENT

X.-Z.L. appreciates the hosting and support from ANSTO during his stay as an Aisa-Oceania Neutron Scattering Association (AONSA) young research fellow. This paper was supported by the National Key Research Program of China (Grant No. 2016YFA0300701), the National Natural Science Foundation of China (Grants No. 11534015, No. 11374347, No. 11505296, and No. 51371192), and the Chinese Academy of Sciences (Grants No. XDB07030200 and No. KJZD-EW-M05).

[1] T. Kimura, T. Goto, H. Shintani, K. Ishizaka, T. Arima, and Y. Tokura, Nature (London) **426**, 55 (2003).
[2] N. Hur, S. Park, P. A. Sharma, J. S. Ahn, S. Guha, and S.-W. Cheong, Nature (London) **429**, 392 (2004).
[3] T. Goto, T. Kimura, G. Lawes, A. P. Ramirez, and Y. Tokura, Phys. Rev. Lett. **92**, 257201 (2004).
[4] N. A. Spaldin and M. Fiebig, Science **309**, 391 (2005).
[5] S.-W. Cheong and M. Mostovoy, Nat. Mater. **6**, 21 (2007).
[6] Y. Yamasaki, S. Miyasaka, Y. Kaneko, J.-P. He, T. Arima, and Y. Tokura, Phys. Rev. Lett. **96**, 207204 (2006).
[7] I. A. Sergienko, C. Sen, and E. Dagotto, Phys. Rev. Lett. **97**, 227204 (2006).

[8] Y. S. Chai, Y. S. Oh, L. J. Wang, N. Manivannan, S. M. Feng, Y. S. Yang, L. Q. Yan, C. Q. Jin, and K. H. Kim, Phys. Rev. B **85**, 184406 (2012).
[9] S. M. Feng, Y. S. Chai, J. L. Zhu, N. Manivannan, Y. S. Oh, L. J. Wang, Y. S. Yang, C. Q. Jin, and K. H. Kim, New J. Phys. **12**, 073006 (2010).
[10] Y. J. Choi, H. T. Yi, S. Lee, Q. Huang, V. Kiryukhin, and S.-W. Cheong, Phys. Rev. Lett. **100**, 047601 (2008).
[11] H. Katsura, N. Nagaosa, and A. V. Balatsky, Phys. Rev. Lett. **95**, 057205 (2005).
[12] I. A. Sergienko and E. Dagotto, Phys. Rev. B **73**, 094434 (2006).
[13] Y. Tokura, S. Seki, and N. Nagaosa, Rep. Prog. Phys. **77**, 076501 (2014).
[14] T. Kimura, G. Lawes, and A. P. Ramirez, Phys. Rev. Lett. **94**, 137201 (2005).
[15] S. Ishiwata, Y. Taguchi, H. Murakawa, Y. Onose, and Y. Tokura, Science **319**, 1643 (2008).
[16] Y. Kitagawa, Y. Hiraoka, T. Honda, T. Ishikura, H. Nakamura, and T. Kimura, Nat. Mater. **9**, 797 (2010).
[17] S. H. Chun, Y. S. Chai, Y. S. Oh, D. Jaiswal-Nagar, S. Y. Haam, I. Kim, B. Lee, D. H. Nam, K.-T. Ko, J.-H. Park, J.-H. Chung, and K. H. Kim, Phys. Rev. Lett. **104**, 037204 (2010).
[18] M. Soda, T. Ishikura, H. Nakamura, Y. Wakabayashi, and T. Kimura, Phys. Rev. Lett. **106**, 087201 (2011).
[19] S. H. Chun, Y. S. Chai, B.-G. Jeon, H. J. Kim, Y. S. Oh, I. Kim, H. Kim, B. J. Jeon, S. Y. Haam, J.-Y. Park, S. H. Lee, J.-H. Chung, J.-H. Park, and K. H. Kim, Phys. Rev. Lett. **108**, 177201 (2012).
[20] F. Wang, T. Zou, L. Q. Yan, Y. Liu, and Y. Sun, Appl. Phys. Lett. **100**, 122901 (2012).
[21] S. Hirose, K. Haruki, A. Ando, and T. Kimura, Appl. Phys. Lett. **104**, 022907 (2014).
[22] S. Shen, L. Yan, Y. Chai, J. Cong, and Y. Sun, Appl. Phys. Lett. **104**, 032905 (2014).
[23] S. Shen, Y. Chai, and Y. Sun, Sci. Rep. **5**, 8254 (2015).
[24] J. Smit and H. P. J. Wijn, *Ferrites* (Phillips Technical Library, Eindhoven, the Netherlands, 1959).
[25] S. Ishiwata, D. Okuyama, K. Kakurai, M. Nishi, Y. Taguchi, and Y. Tokura, Phys. Rev. B **81**, 174418 (2010).
[26] H. B. Lee, Y.-S. Song, J.-H. Chung, S. H. Chun, Y. S. Chai, K. H. Kim, M. Reehuis, K. Prokeš, and S. Mat'aš, Phys. Rev. B **83**, 144425 (2011).
[27] H. Chang, H. B. Lee, Y.-S. Song, J.-H. Chung, S. A. Kim, I. H. Oh, M. Reehuis, and J. Schefer, Phys. Rev. B **85**, 064402 (2012).
[28] H. B. Lee, S. H. Chun, K. W. Shin, B.-G. Jeon, Y. S. Chai, K. H. Kim, J. Schefer, H. Chang, S.-N. Yun, T.-Y. Joung, and J.-H. Chung, Phys. Rev. B **86**, 094435 (2012).
[29] T. Nakajima, Y. Tokunaga, M. Matsuda, S. Dissanayake, J. F. Baca, K. Kakurai, Y. Taguchi, Y. Tokura, and T. Arima, Phys. Rev. B **94**, 195154 (2016).
[30] See Supplemental Material at http://link.aps.org/supplemental/10.1103/PhysRevB.95.094405 for discussion on the microscopic origin of ferroelectricity in the ALC phase and additional measurements of magnetization, ME current, electric polarization, and neutron diffraction.
[31] N. Momozawa, M. Mita, and H. Takei, J. Cryst. Growth **83**, 403 (1987).